Inversion Algorithms for Water Vapor Radiometers Operating at 20.7 and 31.4 GHz

G. M. Resch
TDA Technology Development

Eight water vapor radiometers (WVRs) have been constructed as research and development tools to support the Advanced Systems Program in the Deep Space Network and the Crustal Dynamics Project. These instruments are intended to operate at the stations of the Deep Space Network (DSN), various radio observatories, and mobile facilities that participate in very long baseline interferometric (VLBI) experiments. It is expected that the WVRs will operate in a wide range of meteorological conditions. Several algorithms are discussed that can be used to estimate the line-of-sight path delay due to water vapor and columnar liquid water from the observed microwave brightness temperatures provided by the WVRs. In particular, systematic effects due to site and seasonal variations are examined. The accuracy of the estimation as indicated by a simulation calculation is approximately 0.3 cm for a noiseless WVR in clear and moderately cloudy weather. With a realistic noise model of WVR behavior, the inversion accuracy is approximately 0.6 cm.

I. Introduction

The applications that concern the DSN are contained in the general areas of radio geodesy and spacecraft navigation (Ref. 1). The experimental techniques utilize microwave signals from extraterrestrial radio sources to measure a differential – time of arrival, doppler, or range. Propagation effects imposed by the Earth's atmosphere are treated as unknown time delays or an increase in range and must be calibrated. In this section the water vapor problem is reviewed, and it is noted that the excess path length can be expressed as an integral of the vapor density divided by the temperature integrated along the line of sight. In Section II, the equation of radiative transfer is solved, and it is shown that, given certain assumptions, the brightness temperature or opacity of the atmosphere can be used to estimate the excess path delay due to water vapor. In Section III, a cross section of meteorological data is used to solve for the constants in several formulations of the inversion algorithm, and site and seasonal variations are discussed.

The primary atmospheric propagation effect that concerns the geodesist or navigator is refraction. The apparent or electrical path length L_e, along some atmospheric path L, is defined as

$$L_e = \int_L n(s)\, ds \tag{1}$$

where $n(s)$ is the refractive index at the position s.

As a matter of convenience we will work with the excess path length $\Delta L = L_e - L$ or

$$\Delta L = \int_L (n-1)\, ds \tag{2}$$

Since the refractive index of the atmosphere departs from unity by only a few parts per ten thousand (or less), it is customary to use the refractivity N, defined as

$$N = (n-1)\, 10^6 \tag{3}$$

so that the refractivity of a unit volume is characterized by this number of N units, typically on the order of 320 at sea level. Bean and Dutton (Ref. 2) discuss several formulations of N as a function of atmospheric parameters. Used here is the form given by Smith and Weintraub (Ref. 3),

$$N = 77.6 \left(\frac{P}{T}\right) + 3.73 \times 10^5 \left(\frac{e}{T^2}\right) \tag{4}$$

where P = total pressure (mb), T = temperature (K), and e = partial pressure of water vapor (mb). This expression is considered accurate to 0.5% for frequencies less than 30 GHz in normal ranges of temperature, pressure, and relative humidity. Note that the total refractivity can be written as the sum of a "dry" term $N_d = 77.6\ (P/T)$ and a "wet" term $N_v = 3.73 \times 10^5\ (e/T^2)$ that yields both a dry, ΔL_d, and wet, ΔL_v, path delay correction:

$$\Delta L_d = 77.6 \times 10^{-6} \int \frac{P}{T}\, ds \tag{5}$$

$$\Delta L_v = 3.73 \times 10^{-1} \int \frac{e}{T^2}\, ds \tag{6}$$

The concern here is with the wet term, and elementary definitions (e.g., see Ref. 4) can be used to express the vapor partial pressure as the vapor density ρ_v to get the expression

$$\Delta L_v\ (\text{cm}) = 1.723 \times 10^{-3} \int_L \frac{\rho_v}{T}\, ds \tag{7}$$

where ρ_v is measured in units g/m^3, s is in meters, and a line of sight through the entire atmosphere is assumed. Since water vapor is *not* a well mixed constituent of the atmosphere, ΔL_v will vary according to site, season, and local meteorological conditions. Both the point value of the vapor density and its distribution vertically and horizontally will vary on a variety of time and spatial scales. Zenith values of ΔL_v vary from 3 to 20 cm and scale approximately as the cosecant of the elevation angle for other line-of-sight paths. In applications, observations are not usually made at the zenith but over a wide range of elevation angles for which El = 30° might be an average value. The path delay might therefore vary between 3 and 40 cm as extremes. Clearly, if accuracy goals are on the order of 3 m, water vapor effects can be ignored. If the accuracy goal is 30 cm, somehow the water vapor effect must be estimated but the estimate of ΔL_v does not have to be very good, e.g., if Eq. (7) could be estimated with an accuracy of 50%, the system accuracy requirement might well be satisfied. In order to make this estimate a nominal model of the vapor distribution $\rho_v(s)$ might be used and vertical and horizontal fluctuations might simply be ignored. If the goal is a 3 cm system accuracy, then the temporal and spatial variation of ρ_v along the line of sight is no longer ignorable. The integral in Eq. (7) must be estimated while observing with the geodetic system. Accurate estimates of the line-of-sight path delay must be made from direct measurements or by use of the techniques of remote sensing. In this paper, a microwave technique of passive remote sensing that utilizes a water vapor radiometer (WVR) is described.

When a radio wave from an extraterrestrial source impinges upon the Earth's atmosphere at other than normal incidence, Snell's law tells us that the direction of propagation will be changed. At the Earth's surface, $n \sim 1.0003$ and approaches unity with increasing height so that in general the ray path has a curvature that is concave downward. To an observer on the Earth's surface, an extraterrestrial radio source will appear at a slightly higher elevation than he would calculate from an ephemeris. The difference between the observed elevation of the source and the true elevation is called the angular refraction and represents a rough measure of the curvature in the ray path. At high elevations the curvature is negligible and the path L in Eq. (1) is equivalent to the geometric line of sight to the source. However, at low elevations the path curvature becomes appreciable; Eq. (1) must be expressed in spherical coordinates and is solved using ray tracing methods (e.g., see Ref. 2) which require full specification of the total refractivity in both vertical and horizontal planes. Intuitively, we can see that at low elevations the actual propagation path becomes very dependent upon gradients in the vertical refractivity profile. Most of the refraction occurs in the lowest 10 km of the atmosphere so that a ray entering at say 5° elevation will travel a path whose projected length on the Earth's surface is about 115 km. Even if we knew the distribution of refractivity above the observing site, it is highly unlikely that this distribution would apply along the entire projected path. Depending on our system accuracy requirements, there will be some elevation angle below which these effects defy our current calibration ability. Our current

approach is to avoid these problems by restricting observations to elevation angles greater than 15°.

II. Formulation of the Algorithm

The previous section established the problem as the estimation of the integral quantity

$$\Delta L_v = 1.723 \times 10^{-3} \int \frac{\rho_v}{T} \, ds$$

A suggestion of how this quantity might be estimated can be gotten from consideration of Fig. 1. In this figure is plotted the calculated brightness temperature of a model atmosphere in the frequency range 10 to 40 GHz for three cases. The first case is for a standard atmosphere containing no water, i.e., $M_v = M_L = 0$ where M_v and M_L are the precipitable vapor and liquid, respectively, in units of g/cm^2. The precipitable vapor or liquid is defined as that mass of vapor or liquid that would be precipitated from a column extending through the entire atmosphere with a cross section of 1 cm^2. The second case shows the spectrum of an atmosphere containing $M_v = 2$ g/cm^2 distributed exponentially with a scale height of 2 km. The third case shows the same atmosphere with an additional liquid $M_L = 0.1$ g/cm^2 that is assumed to exist in small droplets. The "bump" in the curves for cases (2) and (3) is due to emission from the water vapor molecule, and it is apparent that the brightness temperatures is a strong function of the amount of water vapor. Thus, a measurement of the brightness temperature is effectively an estimate of the integrated vapor density which constitutes a major portion of the integral in Eq. (7). The problem then is to find the explicit form of the relationship between brightness temperature and vapor path delay and to subtract out the effect of liquid water. In order to do this, the techniques of passive remote sensing will be used.

We will consider the emission and absorption properties of the atmosphere in terms of a gaseous medium in local thermodynamic equilibrium. For a nonscattering, nonrefractive medium, the equation of radiative transfer given by Chandrasekhar (ref. 5) can be transformed using the Rayleigh-Jeans approximation of Planck's law of radiation to the form,

$$T_b(s) = T_b(0) \exp\left[-\tau(s, o)\right] + \int T(s)\, \alpha(f, s) \exp\left[-\tau(s, s')\right] ds \qquad (8)$$

which is shown schematically in Fig. 2. Radiation at a frequency f, of apparent blackbody temperature $T_b(s)$ is detected at position s from a medium that both emits and absorbs. Radiation $T_b(0)$ is incident on the medium at $s = 0$ and is attenuated by the factor $\exp\left[-\tau(s, o)\right]$. A unit volume of the medium at a physical temperature $T(s)$, characterized by an absorption coefficient $\alpha(f, s)$ will emit radiation at frequency f, which is attenuated by the factor $\exp\left[-\tau(s, s')\right]$. The optical thickness τ (or opacity) is defined as

$$\tau(s, s') = \int_s^{s'} \alpha(f, s'')\, ds'' \qquad (9)$$

By the mean value theorem of integral calculus the integral in Eq. (8) can be written

$$\int T \alpha \exp(-\tau)\, ds = T_M \int \alpha \exp(-\tau)\, ds \qquad (10)$$

where T_M is termed the mean radiating temperature of the atmosphere. Using this definition the solution to Eq. (8) is

$$T_b = T_c \exp(-\tau) + T_M \left[1 - \exp(-\tau)\right] \qquad (11)$$

For low values of the opacity ($\tau \ll 1$) $T_b \sim T_c$, i.e., the medium is transparent and we simply "see" the incident radiation which in this case is T_c, the cosmic blackbody background at an apparent temperature of 2.9 K. For large values of the opacity ($\tau \gg 1$) $T_b \sim T_M$, the medium is opaque and we "see" the gas radiating at its effective temperature. It is convenient to solve Eq. (11) for the opacity in the form

$$\tau = -\log_e \left(\frac{T_M - T_b}{T_M - T_c} \right) \qquad (12)$$

We can express the total atmospheric absorption in Eq. (9) as the sum of its three primary contributors, a water vapor term, α_v, a liquid term, α_L, and a "dry" term, α_d, that describes the background radiation primarily from the wings of a series of oxygen resonance lines near 60 GHz:

$$\tau = \int (\alpha_v + \alpha_L + \alpha_d)\, ds = \tau_v + \tau_L + \tau_d \qquad (13)$$

Explicit formulations of the absorption coefficients can be found in the literature. This study uses Waters' form of the water vapor absorption coefficient (Ref. 6), Snider and Westwater's form for oxygen (Ref. 7), and Staelin's form for liquid water (Ref. 8). Since the water vapor absorption is a

linear function of the vapor density we can write the vapor opacity term as

$$\tau_v = \int \left(\frac{\rho_v}{T}\right)\left(\frac{\alpha_v T}{\rho_v}\right) ds \tag{14}$$

Thus, the opacity due to water vapor can be expressed in a form that contains the functional form (i.e., Eq. [7]) of the path delay integral.

To express the vapor opacity as a linear function of the path delay, $\tau_v = G(\Delta L_v)$ where G should be constant with respect to s but may be a function of frequency f, implies

$$G(f, s) = (5.803 \times 10^2)\left(\frac{\alpha_v T}{\rho_v}\right) \tag{15}$$

Let us suppose that we measure the brightness temperature at two frequencies f_1 and f_2 and transform the observables T_{b1}, T_{b2} using Eq. (12) to estimate the total opacity. At each frequency Eq. (12) can be written

$$\tau_1 = G_1(\Delta L_v) + \tau_{L1} + \tau_{d1} \tag{16}$$

$$\tau_2 = G_2(\Delta L_v) + \tau_{L2} + \tau_{d2} \tag{17}$$

Staelin (Ref. 8) has given an expression for the absorption coefficient for liquid water which varies as frequency squared so that $\tau_L = kf^2$, or $\tau_{L2} = (f_2/f_1)^2\, \tau_{L1}$. In a similar manner the dry opacities scale by frequency according to $\tau_{d2} = \beta(f_2/f_1)^2\, \tau_{d1}$, where the parameter β depends on f_1 and f_2. Thus, Eq. (17) is transformed to

$$\tau_2 = G_2(\Delta L_v) + \left(\frac{f_2}{f_1}\right)^2 \left(\tau_{L1} + \beta\, \tau_{d1}\right) \tag{18}$$

which, together with Eq. (16), can be solved to give

$$\Delta L_v = \left[G_1 - \left(\frac{f_1}{f_2}\right)^2 G_2\right]^{-1} \times \left[\tau_1 - \left(\frac{f_1}{f_2}\right)^2 \tau_2 - (1-\beta)\,\tau_{d1}\right] \tag{19}$$

$$\tau_{L1} = \left[G_2 - \left(\frac{f_2}{f_1}\right)^2 G_1\right]^{-1} \times \left[G_2\,\tau_1 - G_1\,\tau_2 - \left(G_2 - \beta\left[\frac{f_2}{f_1}\right]^2 G_1\right)\tau_{d1}\right] \tag{20}$$

As we did with the vapor term, we can assume that $\tau_L = Z_L M_L$, where Z_L is the weighting function for liquid water, and M_L is the precipitable liquid. Thus,

$$M_L = \left[G_2 - \left(\frac{f_2}{f_1}\right)^2 G_1\right]^{-1} \times \left[G_2\,\tau_1 - G_1\,\tau_2 - \left(G_2 - \beta\left[\frac{f_2}{f_1}\right]^2 G_1\right)\tau_{d1}\right] Z_L \tag{21}$$

Equations (19) and (21) represent the formal solutions for the excess path delay due to water vapor ΔL_v, and the integrated liquid content M_L, in terms of the transformed observables τ_1 and τ_2 defined by Eq. (12).

If we are able to measure the brightness temperatures T_{b1} and T_{b2}, then in principle we can estimate the vapor path delay ΔL_v and integrated liquid content M_L. The accuracy of these estimates is limited by our ability to measure the brightness temperatures and the quality of our assumptions, namely, (1) that the quantities T_M, G_1, G_2, τ_{d1}, and Z_L are constant and (2) that the radiation from liquid water varies as f^2. Accurate measurement of T_b is primarily an instrumental calibration problem. In the next section the overall quality of these assumptions is examined directly.

III. Determination of Constants in the Algorithm

In order to use the inversion algorithms given in Eqs. (19) and (21), we must determine the mean radiating temperature of the atmosphere, the vapor weighting functions, the liquid weighting function, and the opacity due to the dry component of the atmosphere. These quantities have been assumed to be constant in the derivation of the algorithm, but in a real atmosphere they exhibit variation and correlation with other atmospheric parameters. While these variations are not so

large as to invalidate the basic assumptions, they clearly indicate some level of error in the algorithm. This implies that we must always expect some level of "algorithm noise," and our efforts must be directed towards its reduction. Furthermore, some fraction of this algorithm noise is likely to represent systematic variations that are a function of site and season. If we were given a meteorological history of each WVR site, we might be able to develop the constants in our algorithms in such a way that would be optimized for that site and hopefully reduce the seasonal variations. However, this procedure presents potential operational problems: (1) The meteorological history may not be available or easy to obtain; (2) it is a fair amount of work if there are many sites (e.g., as with mobile VLBI); and (3) someone must keep careful track of which algorithm goes with a particular site, and if that someone mixes the algorithms, the error could be compounded. A far simpler procedure would be to derive a single formulation of the algorithm in which the "constants" were no longer constant but instead some simple function of site and seasonal parameters, i.e., in effect we would use a model to reduce the site and seasonal systematic errors in the algorithm. Any WVR user must decide on which approach to use based on his accuracy requirements as well as cost and operational reliability. The interpretation adopted here is to use a single algorithm for all sites and to demonstrate that the residual site and season dependencies are less that the currently required level of accuracy.

We can best evaluate the level of algorithm noise as well as site and seasonal variations by determining the constants in a given formulation of the algorithm by using a regression analysis. That is, we will use meteorological data (e.g., radiosonde data) to compute the path delay and to solve the equation of radiative transfer for the associated brightness temperatures at 20.7 and 31.4 GHz for a relatively large number of cases. This data base will then be used to determine the value of the constants in an inversion algorithm that will minimize the residuals in a least squares sense. Of course, as a practical matter, we will still be left with the problem of relating the temperature scale of our WVRs to the temperature scale defined in Eq. (8). Since our knowledge of fundamental quantities like the absorption coefficients as well as our calibration of the radiometers will always be less than perfect, we must accept the fact that ultimately the WVRs must be compared directly with some independent method of measuring path delay if we wish an absolute calibration.

A data base of radiosonde data was assembled from five sites in the United States during the year 1976. The sites – Portland, Maine; Pittsburgh, Pennsylvania; El Paso, Texas; San Diego, California; and Oakland, California – were chosen to represent a cross section of meteorological conditions. Each radiosonde launch provides an approximately vertical profile of pressure, temperature, and relative humidity that is used to calculate the vapor path delay and to numerically solve the equation of radiative transfer for the brightness temperature, mean radiating temperature, and the opacity. One launch out of eight was selected from each site so as to obtain equal amounts of data from both 0 and 12 hours Universal Time and to cover seasonal trends in the data. Thus, for each radiosonde site we have 92 values of the vapor path delay ΔL_{vi} and 92 pairs of brightness temperatures $T1_i$ (20.7 GHz) and $T2_i$ (31.4 GHz). We use the latter to estimate the path delay $\langle \Delta L_v \rangle_i = f(T1_i, T2_i)$ and in a straightforward manner solve for the constants in any given functional form $f(T1_i, T2_i)$ that minimizes the difference $\Delta L_{vi} - \langle \Delta L_v \rangle_i$, in a least squares sense.

The radiosonde data does not provide any direct indication of the presence or amount of liquid water. As we noted previously, the presence of even small amounts of liquid (as in clouds) has a pronounced effect on the brightness temperatures measured by the WVR. Hence, it is essential that we evaluate the performance of the vapor retrieval algorithm in the presence of liquid. In order to simulate the presence of clouds the data from each radiosonde launch are scanned for an indication that the relative humidity is greater than 95%, which we assume indicates an equilibrium condition with liquid. The points at which the relative humidity falls below 94% define the top and bottom of the cloud, and the altitude of these points is calculated by simple linear interpolation. Given the cloud thickness and altitude, we use all three of the models for the cloud liquid density given by Decker *et al.* (Ref. 9) which we denote by CMODEL = 1, 2, or 3 (CMODEL = 0 denotes no liquid). The temperature of the liquid was taken to be the interpolated temperature of the radiosonde in the cloud, and the absorption coefficient of liquid water given by Staelin (Ref. 8) is used to calculate the brightness temperature. Using this criterion, a total of 121 radiosonde launches from the 5 sites was found that suggests the presence of liquid water. Thus, for each cloud model there were 121 values of the precipitable liquid M_{Li}, and 121 pairs of observables $T1_i$ and $T2_i$. The regression analysis for the liquid water retrieval then proceeds in a manner that is completely analogous to analysis used for the vapor algorithm. For the vapor algorithm, the constants are derived in the regression analysis using clear-sky data and tested with the cloud data. For the liquid algorithm, the constants are derived with the cloud data and tested with the clear-sky data.

Generally, the zenith brightness temperature in clear-sky conditions at both of our frequencies will be less than 50 K and the corresponding opacity less than 0.2 neper. This suggests that we could expand the logarithm in Eq. (20) and keep only the first order term in T_b, i.e., a low opacity approx-

imation. The estimated path delay would then be of the form

$$\langle \Delta L_v \rangle_i = A_0 + A_1 \, [T1 - 0.4346 \times T2]_i \qquad (22)$$

where $T1$ and $T2$ are the brightness temperatures at 20.7 and 31.4 GHz, respectively. Table 1 summarizes the best fit parameters for this estimate. First, note that since we are using noise free data, the RMS of the fit represents the quality of the assumptions that have gone into the estimate, i.e., "algorithm noise." We would expect a larger RMS than shown if we actually compared WVR data with real radiosondes for in that case we would be comparing two noisy observables and the RMS would represent the quadratic sum of the radiosonde error and WVR error. Second, note that the values of the "constants" A_0 and A_1 vary from site to site by more than their standard errors, clearly indicating systematic effects are present in the data. This is further emphasized by the fact that the RMS of the fit for all sites is larger than the RMS from any single site. Progressive degradation of the algorithm can be seen in the increasing RMS under cloudy conditions, i.e., increasing opacity. Analysis of the residuals indicates that they correlate with surface values of the pressure, temperature, and the opacity. Of these correlations the opacity is by far the most important. Since our data base represents only zenith values, both the variation and the absolute values of the opacity tend to be small. In a real experiment, the WVR may be pointed down to an elevation angle of ~15° and the range of opacities will vary accordingly. Still, the RMS of the fit for all sites is not too bad so that Eq. (22), since it is particularly simple, is adequate for a quick estimate of the delay.

In order to obtain some idea as to the performance of our algorithms in actual operation, we must know the instrumental noise spectrum imposed on the observables and must include an estimate of its magnitude in the regression analysis. One method that can be used to estimate the instrumental stability is to have two side-by-side radiometers observe the same target, e.g., the sky, and note the difference between the two brightness temperatures. In principal, this difference should appear to be Gaussian noise with an RMS equal to $\sqrt{2}$ times the RMS fluctuations of a single radiometer and can be reduced by simply increasing the integration time. In reality, the integration time can only be increased to the point where the inevitable systematic errors begin to predominate. Data taken during the testing and calibration of the WVRs indicate that the noise spectrum is "white" on time scales less than ~3 h and therefore can be reduced by averaging. For time scales greater than 3 h, flicker noise seems to predominate and appears as a slow drift of the antenna temperature about some nominal value with an amplitude of ±1 K. Since the geodetic experiments that we expect to support are normally longer than 3 h, we will model the radiometer noise with a uniformly distributed random variable drawn from the interval ±1 K, added to the brightness temperature. The regression analysis then proceeds as in the noise-free case. Differences in the RMS of the fit between the noisy and noise-free data indicate the relative importance on instrumental noise and systematics in the algorithm.

The simple formulation in Eq. (22) does not take into account that radiation from distant vapor along the line of sight is attenuated by intervening vapor. This correction is done explicitly by using the opacity as the transformed observable. Table 2 summarizes the best fit parameters for the path delay estimate that now includes the transformation to opacity given by Eq. (12) (where T_m = 275 K). Except for the El Paso data set, we see that the constants are reasonably consistent from site to site. Although there is a small bias for the cloud liquid data, the RMS of the estimate in the presence of liquid is consistent with the clear sky data – a definite improvement over the previous algorithm. When a uniformly distributed ±1 K of noise is added to the brightness temperatures, the RMS for all sites rises to 0.55 cm, indicating roughly equal contributions from algorithm noise and instrumental systematics. This form of the algorithm is useful in circumstances where measurements of surface temperature and pressure are not readily available.

When values of the surface pressure and temperature are available, we can use them to further refine our algorithm. The next most obvious parameter to model is the mean radiating temperature T_M. Figure 3 illustrates the frequency dependence of T_M in a plot of T_M versus frequency for a standard atmosphere containing an exponential distribution of water vapor with total columnar content M_v = 2 g/cm^2. Figure 4 shows how T_M varies as a function of M_v, again in a standard atmosphere. The mean radiating temperature is also a function of the physical temperature distribution in the atmosphere and will exhibit site and seasonal variation. Figure 5 illustrates this variation for the Portland, Maine, data for the year 1976, and Table 3 summarizes the statistics of both T_M and the surface temperature T_S. The RMS variations in T_M indicated in Table 3 suggest that this could be a significant error source in the inversion algorithm, and some effort is warranted to reduce this variation. If we assume a simple linear relationship between T_M and the surface temperature T_s, then the estimates

$$T_{M1} = 50.3 + 0.786\, T_s \qquad (f = 20.7 \text{ GHz}) \qquad (23)$$

$$T_{M2} = T_{M1} + 3.4 \qquad (f = 31.4 \text{ GHz}) \qquad (24)$$

reduce the RMS variation of T_M from all sites by a factor of two. Table 4 summarizes the best linear fit between T_M and the surface temperature T_S for each site. Note that the RMS for all sites in Table 4 is larger than the RMS for any individual site. This strongly suggests that this simple linear fit does not completely remove all site-to-site and/or seasonal variations. However, these equations do reduce the RMS to an acceptable level and have the virtue of being simple to use – a significant consideration if one must deal with data from many sites.

For the next formulation of an algorithm, we will model the mean radiating temperatures T_{M1} and T_{M2} and assume that the dry opacity scales as the surface pressure squared times the surface temperature to the -2.86 power. The multiplier of the dry opacity term will be chosen to force the bias term, i.e., A_0, to be zero. The algorithm that we shall now fit then takes the form

$$\langle \Delta L_v \rangle = A_0 + A_1 \left[\tau_1 - 0.4346\, \tau_2 - \left(\frac{A_2}{A_1}\right) \left(\frac{P_s}{1013}\right)^2 \times \left(\frac{293}{T_s}\right)^{2.86} AM \right] \tag{25}$$

where we have included the air mass scaling for the dry term, i.e., AM = cosecant (elevation). The opacity at frequency F_i is

$$\tau_i = -\log_e \left(\frac{T_{mi} - T_{bi}}{T_{mi} - T_c} \right) \tag{12}$$

where T_{m1} is given by Eq. (23) and T_{m2} by Eq. (24). Table 5 summarizes the regression analysis for this algorithm. We see that the RMS and the site-to-site consistency is a bit better than the previous algorithm and the performance in the presence of liquid is about as good. If surface measurements are available, we would prefer this algorithm to the previous formulation, but note that the accuracy of either meets the calibration requirements of the Crustal Dynamics Project. When noise is added to the RMS, the fit for all sites rises to 0.48 cm and the small site-to-site differences are blurred by larger sigmas on each of the constants.

Since the path delay due to liquid is $\Delta L_L \sim 1.6\, M_L$ (for both ΔL_L and M_L in cm) and M_L is rarely larger than a few millimeters, we see that the liquid delay is considerably smaller than the errors in the vapor estimate. The primary reason for a liquid estimate is not for direct geodetic calibration so much as it is an indicator of WVR performance. We can rewrite Eq. (21) in the form

$$M_L = A_0 + A_1 \left[\tau_2 + \left(\frac{A_2}{A_1}\right) \tau_1 + \left(\frac{A_3}{A_1}\right) \tau_d \right] \tag{26}$$

The value of (A_2/A_1) is found either from calculation of the weighting functions or a multiple regression analysis on the radiosonde data base to be (A_2/A_1) = -0.366. We will use the same functional dependence for the dry term as we used in the vapor algorithm and require the value of (A_3/A_1) to be such as to minimize the value of A_0, i.e., we will minimize the bias term. Table 6 shows the parameters for the best fit solution for this formulation. As we required, the bias term A_0 is less than its standard error for each cloud model and can be taken as effectively zero. When this is done and the liquid water algorithm is used with the main radiosonde data base (where we assumed there was no liquid water), the average residual at each site is comfortably small with an RMS value comparable to the retrieval accuracy in the liquid data set. Note that units have switched to micrometers for the liquid measure. The increasing RMS of the retrieval with cloud model suggests that the accuracy of the liquid retrieval is a function of the liquid density. Figure 6 shows the average precipitable liquid versus the RMS of the retrieval for each site and each cloud model. The error in the liquid water estimate suggested by this data is

$$\mathrm{RMS}\,(M_L) = 0.32 \times M_L \tag{27}$$

When we include the WVR error model in the regression analysis for liquid retrieval, the RMS of fit changes relatively little and suggests that the retrieval accuracy is limited by the algorithm. In fact, the algorithm for the liquid water estimate contains relatively more error than the vapor algorithm due to the fact that the liquid weighting function contains an exponential dependence on the liquid temperature (Ref. 8), which is not an easily modeled quantity. The presence of liquid water during a tip-curve calibration observation is an immediate indication that the tip-curve data will be noisy and should be weighted accordingly. If we are observing in clear sky conditions and the WVR reports a nonzero (i.e., greater than the RMS value) amount of liquid water, it suggests that either the radiometric temperature scales needs recalibration or the vapor weighting functions are very different than the "average" weighting function determined by earlier analysis. The latter possibility could be due to an unusual vertical profile of vapor although we have chosen the vapor sensitive frequency to minimize this type of error. Finally, the presence of large amounts of liquid or equivalently, large values of opacity at 31.4 GHz, indicate that an important assumption in our derivation may be violated. In large concentrations of liquid, the drop size tends to grow and scattering plays an increasingly important part in the apparent radiation spectrum. When the effective diameter

of the drop is on the order of the observing wavelength, the scattering process is termed Mie scattering, and the spectrum is more complex than the simple Rayleigh scattering that we have assumed. The radiation spectrum of large drops can no longer be characterized by a simple power-law-type behavior, which means that both our vapor and liquid algorithms break down. Since the breakdown is primarily a function of the drop size distribution of the liquid, there is no clear criterion that distinguishes the operating from the nonoperating regimes of the algorithm. Westwater (Ref. 10) and Westwater and Guiraud (Ref. 11) estimate that these remote sensing techniques are applicable up to opacities of 3 db = 0.7 neper (at 31 GHz). Given the considerable observing experience of these experimenters, this is probably the best operating/nonoperating criterion that can presently be stated.

IV. Summary

Several reasonably simple algorithms have been derived that relate observables, i.e., the brightness temperatures measured with a two-channel WVR, to the line-of-sight path delay that is required to correct various types of radiometric data for the effects of atmospheric water vapor. The three formulations that can be used to estimate the excess path delay due to atmospheric water vapor ΔL_v, are

$$\langle \Delta L_v \rangle = -1.6 + 0.65\,(T_1 - 0.435\,T_2) \tag{28}$$

for convenience. A better algorithm if no surface measurements are available would be

$$\langle \Delta L_v \rangle = 158\,(\tau_1 + 0.435\,\tau_2) \tag{29}$$

where the opacity τ, is

$$\tau_i = -\log_e \left[\frac{275 - T_i}{272}\right] \tag{30}$$

When surface measurements are available, use

$$\langle \Delta L_v \rangle = 164 \left[\tau_1 - 0.435\,\tau_2 - 0.0016 \times \left(\frac{P_s}{1013}\right)^2 \left(\frac{293}{T_s}\right)^{2.86}\right] \tag{31}$$

where the opacity is now

$$\tau_i = -\log_e \left[\frac{T_{Mi} - T_i}{T_{Mi} - T_c}\right] \tag{32}$$

and the quantities T_{Mi} are given in Eq. (23) and (24).

The regression analysis indicates that the ultimate accuracy of the two-channel technique is about 0.2 to 0.3 cm, and with a realistic noise model of the current generation of instruments a 0.5 cm accuracy is possible. Note that the question of radiosonde accuracy is irrelevant in this analysis: It simply represents the "truth." However, if the WVRs are to be compared directly to radiosondes, then the question of radiosonde accuracy is crucially important. Indeed, the WVR's must eventually be calibrated on an absolute scale, and radiosondes seem to be the most cost-effective way to accomplish this at the present time. Consider that such a direct comparison is made at each of the radiosonde launch sites that were used in this analysis. If we assume an average zenith path delay of 10 cm and the measurement accuracy of the radiosonde is 10%, then the RMS of the radiosonde/WVR comparison would be,

$$(1.0)^2 + (0.5)^2 = 1.12 \text{ cm}$$

While it is important to do such a comparison so as to investigate the possibility of a bias term in the inversion, the analysis suggests that the WVR is more accurate than the radiosonde. Hence, the comparison must be done with great caution when attempting improvements in the WVR instrumentation or refinements in the algorithm. We are faced with a recurring problem – how to demonstrate a new measurement technique is as good as we think it is when it is better than any existing technique.

References

1. Resch, G. M. (1980), "Water vapor: The wet blanket of microwave interferometry," eds., Deepak, Wilkerson, and Ruhnke, *Atmospheric Water Vapor*, Academic Press, New York.

2. Bean, B. R., and E. J. Dutton (1968), *Radio Meteorology*, Dover Publ., New York, N.Y.

3. Smith Jr., E. K., and S. Weintraub (1953), "The constants in the equation for atmospheric refractive index at radio frequencies," *Proc. I.R.E.*, Vol. 41, pp. 1035-1057.

4. Hess, S. L. (1959), *Introduction to Theoretical Meteorology*, Holt, Rinehart & Winston, New York.

5. Chandrasekhar, S. (1950), *Radiative Transfer*, Oxford Univ. Press, New Jersey.

6. Waters, J. W. (1976), "Absorption and emission by atmospheric gases," ed., M. L. Meeks, *Methods of Experimental Physics: Astrophys.*, Part B, 12, pp. 142-175.

7. Snider, J. B., and E. R. Westwater (1969), "Atmospheric attenuation at 15, 31, and 53 GHz," *ESSA Tech. Rept. ERL 156-WPL 11*, Dec. 1969.

8. Staelin, D. H. (1966), "Measurements and interpretation of the microwave spectrum of the terrestrial atmosphere near 1-cm wavelength," *J. Geophys. Res., 71*, pp. 2875-2882.

9. Decker, M. T., E. R. Westwater, and F. O. Guiraud (1978), "Experimental evaluation of ground-based microwave radiometric sensing of atmospheric temperature and water vapor profiles," *J. Appl. Meteor., 17*, pp. 1788-1795.

10. Westwater, E. R. (1978), "The accuracy of water vapor and cloud liquid determinations by dual-frequency ground based microwave radiometry," *Radio Science, 13*, pp. 677-685.

11. Westwater, E. R., and F. O. Guiraud (1980), "Ground-based microwave radiometric retrieval of precipitable water vapor in the presence of clouds with high liquid content," *Radio Science, 15*, pp. 947-957.

Table 1. Summary of best fit parameters for a vapor algorithm involving brightness temperature

$$\langle \Delta L_\nu \rangle = A_0 + A_1 \{T1 - 0.4346\, T2\}$$

(no measurement noise)

Cloud Model = 0					
Site	A_0	σ	A_1	σ	RMS, cm
Portland	−1.57	0.05	0.662	0.003	0.28
Pittsburgh	−1.45	0.05	0.649	0.003	0.25
El Paso	−1.39	0.06	0.610	0.004	0.26
San Diego	−1.71	0.13	0.642	0.007	0.38
Oakland	−1.63	0.13	0.644	0.007	0.35
All sites	−1.62	0.05	0.646	0.002	0.41

Cloud Model	Average Residual	RMS
1	0.29	0.45
2	0.20	0.58
3	−0.26	1.55

Table 2. Summary of best fit parameters for a vapor algorithm involving the opacities

$$\langle \Delta L_\nu \rangle = A_o + A_i \{\tau_1 - 0.4346\, \tau_2\}$$

$$\tau_i = -\log_e\left(\frac{275 - TA_i}{272}\right)$$

Cloud Model = 0					
Site	A_0	σ	A_1	σ	RMS[a], cm
Portland	0.01	0.04	160.5	0.6	0.24 (.49)
Pittsburgh	0.08	0.05	158.3	0.7	0.24 (.45)
El Paso	−0.03	0.05	151.4	0.9	0.25 (.45)
San Diego	−0.07	0.11	156.9	1.6	0.37 (.54)
Oakland	−0.07	0.10	158.6	1.7	0.32 (.53)
All sites	−0.06	0.03	157.9	0.5	0.36 (.55)

Cloud Model	Average Residual	RMS[a]
1	0.18	0.35 (.56)
2	0.17	0.35 (.51)
3	0.14	0.37 (.60)

[a]Numbers in parenthesis indicate the RMS with an added noise of ±1 K in each channel.

Table 3. The average mean radiating temperature, the surface temperature, and their RMS values (f = 20.7 GHz)

Site	T_M	RMS	T_S	RMS
Portland	269.4	11.4	279.1	10.8
Pittsburgh	270.3	10.9	281.5	11.3
El Paso	275.2	7.0	289.5	6.0
San Diego	280.1	5.1	290.6	5.7
Oakland	278.0	5.3	287.7	6.0
All sites	274.7	9.4	285.7	10.5

Table 4. Estimates of the mean radiating temperature from the surface temperature ($T_{m1} = A_0 + A_1 T_S$, f = 20.7 GHz)

Site	A_0	A_1	RMS
Portland	6.6	0.94	4.2
Pittsburgh	15.3	0.91	3.7
El Paso	121.8	0.53	3.9
San Diego	86.1	0.67	3.4
Oakland	110.7	0.58	3.9
All sites	50.2	0.786	4.5

Table 5. Summary of best fit parameters for a vapor algorithm involving opacities and surface data

$$\langle \Delta L_\nu \rangle = A_0 + A_1 \left\{ \tau_1 - 0.4346\, \tau_2 - 0.0016\, \tau_d \right\}$$

where

$$\tau_i = -\log_e \left(\frac{T_m - TA_i}{T_m - T_c} \right)$$

$$T_{m1} = 50.3 + 0.786 \times T_s$$

$$T_{m2} = T_{m1} - 3.4$$

$$\tau_d = \left(\frac{P_s}{1013} \right)^2 \left(\frac{293}{T_s} \right)^{2.86}$$

Cloud Model = 0					
Site	A_0	σ	A_1	σ	RMS[a], cm
Portland	0.07	0.03	165.4	0.5	0.18 (.45)
Pittsburgh	0.11	0.03	165.1	0.5	0.16 (.44)
El Paso	−0.05	0.03	159.4	0.5	0.14 (.39)
San Diego	−0.03	0.09	163.7	1.3	0.30 (.47)
Oakland	0.05	0.09	163.9	1.5	0.27 (.44)
All sites	−0.001	0.03	163.9	0.4	0.28 (.48)

Cloud Model	Average Residual	RMS[a]
1	0.13	0.30 (.46)
2	0.19	0.34 (.54)
3	0.29	0.50 (.63)

[a]Numbers in parenthesis indicate RMS with an added noise of ±1 K to each channel.

Table 6. Summary of best fit parameters (μm) for a liquid water algorithm

$$\langle M_L \rangle = A_0 + A_1 (\tau_2 - 0.366, \tau_1 - 0.022\, \tau_d)$$

All Sites Cloud Model	A_0	σ	A_1	σ	RMS[a]
1	−0.3	2.8	5368	107	24 (26)
2	+8.4	12.1	5352	119	105 (108)
3	+26.7	25.7	5279	125	224 (223)

Cloud Model = 0 (no liquid)

Site	Average Residual	RMS[a]
Portland	0.6	33.0 (34)
Pittsburgh	0.3	25.0 (34)
El Paso	11.8	9.6 (15)
San Diego	−7.2	15.6 (22)
Oakland	−3.6	12.7 (17)
All sites	0.3	21.8 (25)

[a]Numbers in parenthesis indicate RMS with an added noise of ±1 K to each channel.

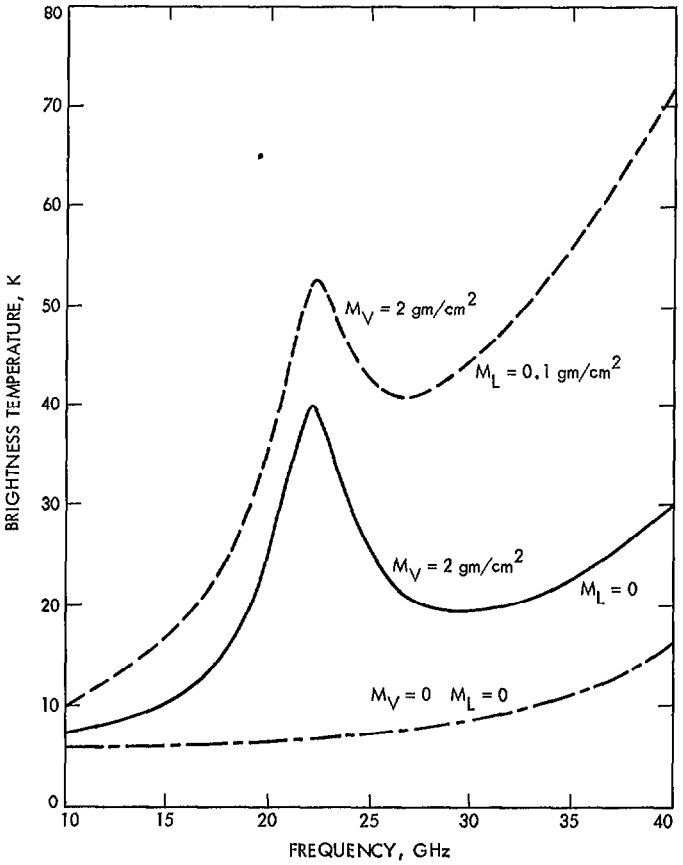

Fig. 1. The zenith brightness temperature of a standard atmosphere for three cases: (1) no water vapor and no liquid water, (2) 2 g/cm^2 of vapor and no liquid, and (3) 2 g/cm^2 of vapor and 0.1 g/cm^2 of liquid

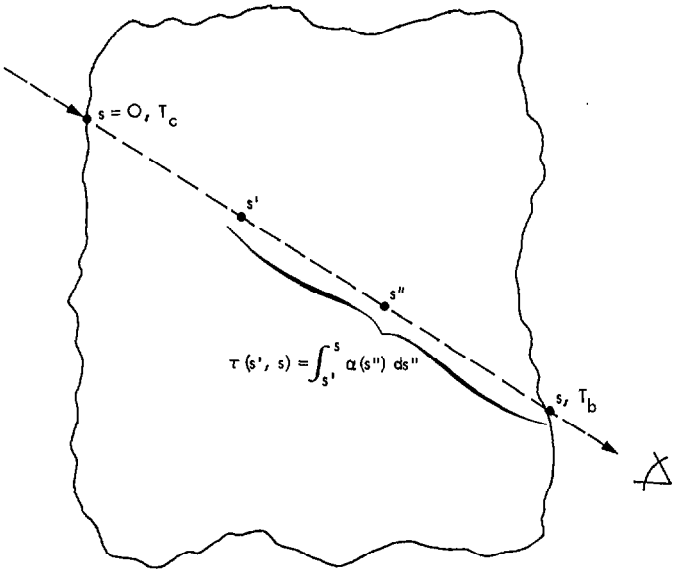

Fig. 2. Schematic representation of the equation of radiative transfer

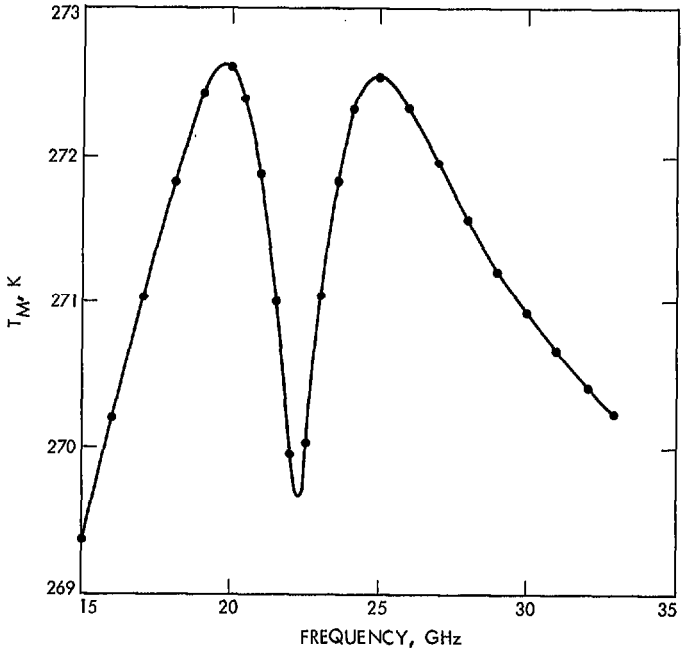

Fig. 3. The mean radiating temperature of a standard atmosphere T_M vs. frequency for M_v = 2 g/cm^2 exponentially distributed in a standard atmosphere

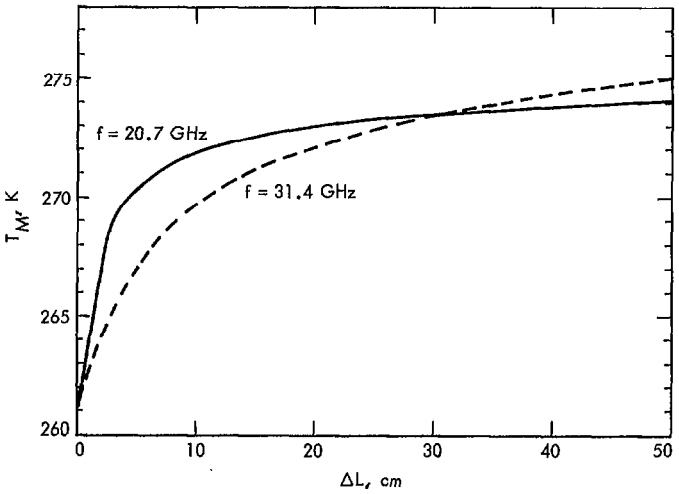

Fig. 4. T_M vs. M_v for f = 20.7 and 31.4 GHz in a standard atmosphere

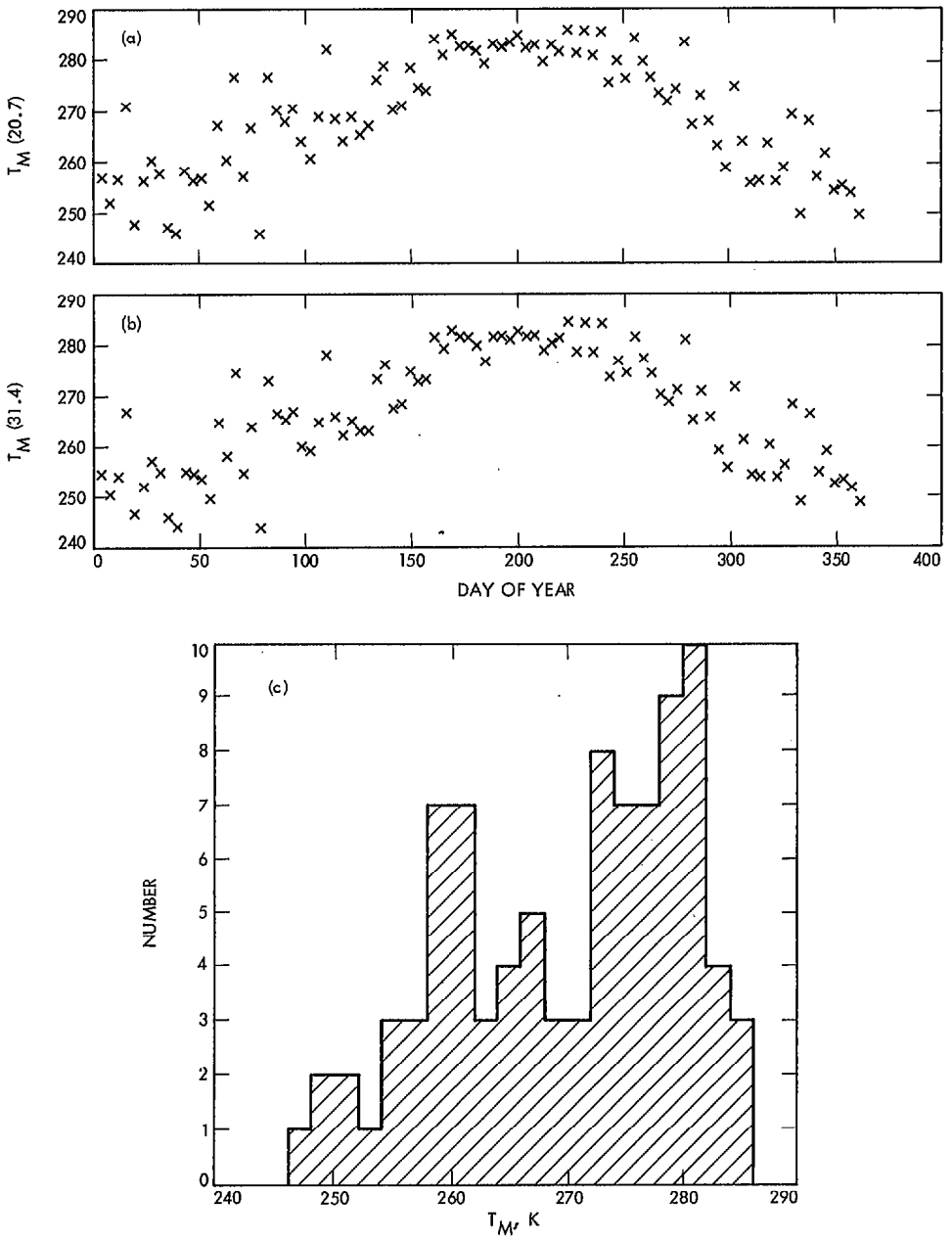

Fig. 5. Portland, Maine, radiosonde data showing (a) T_M vs. time at f = 20.7 GHz; (b) T_M vs. time at f = 31.4 GHz; and (c) the histogram of T_M at 20.7 GHz

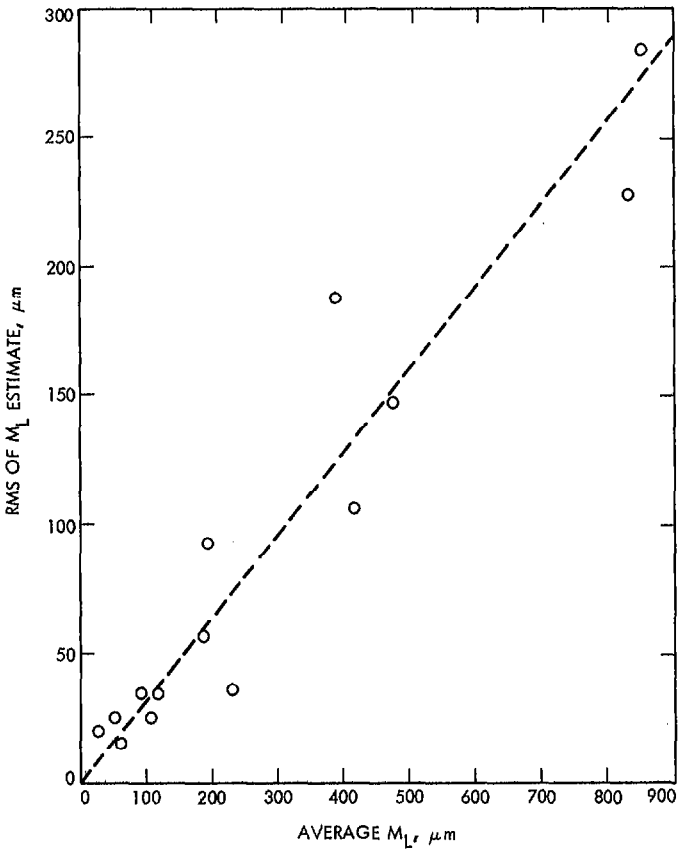

Fig. 6. The RMS of the liquid water retrieval vs. M_L, the precipitable liquid along the line of sight